Fuel 118 (2014) 100–106

Contents lists available at ScienceDirect

Fuel

journal homepage: www.elsevier.com/locate/fuel

Purified hydrogen from synthetic biogas by joint methane dry reforming and steam-iron process: Behaviour of metallic oxides and coke formation

J. Plou, P. Durán, J. Herguido, J.A. Peña *

Catalysis, Molecular Separations and Reactor Engineering Group (CREG), Aragon Institute of Engineering Research (I3A), Universidad Zaragoza, Mariano Esquillor s/n, Ed. "I+D", 50018 Zaragoza, Spain

HIGHLIGHTS

- Production of purified hydrogen starting from synthetic biogas by joint MDR and steam-iron.
- Low heating power biogas has been simulated by equimolar mixtures of CH_4 and CO_2.
- Solid composed of nickel catalyst and doped iron ores as reactive material.
- TG + MS to determine relation between exhaust gas and mass gain/loss of solid.
- Insight over reactions sequence, carbon deposition and self-gasification.

GRAPHICAL ABSTRACT

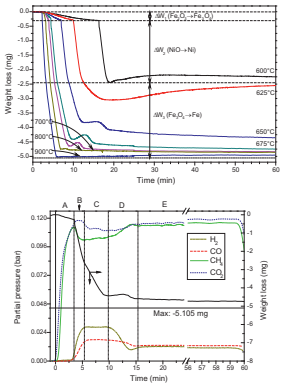

ARTICLE INFO

Article history:
Received 23 July 2013
Received in revised form 18 October 2013
Accepted 29 October 2013
Available online 8 November 2013

Keywords:
Biogas
Dry-reforming
Steam-iron
Hydrogen
Chemical-looping

ABSTRACT

Mechanical mixtures of nickel oxide and iron oxide doped with small quantities of ceria and alumina (2 wt%), have been tested as suitable solids to jointly produce and purify hydrogen from an equimolar mixture of CH_4 and CO_2 simulating a desulfurized biogas. Since the solid mixture constitutes a reactant within the system, most part of the experiments has been carried out in a thermogravimetric system acting as a differential reactor. Exhaust gases were continuously monitored by mass spectrometry at the exit of the thermobalance. The apparent reaction mechanism consists of a first stage in which CH_4 reduces Fe_2O_3 (hematite) to Fe_3O_4 (magnetite) and NiO to metallic Ni. This newly formed metallic nickel adopts a catalytic role promoting the methane dry reforming (MDR) reaction between CH_4 and CO_2. Fe_3O_4 reduces to metallic iron (Fe^0) at the expense of H_2 and CO (products of MDR), that transform in the oxidized species H_2O and CO_2 respectively. This reaction displaces dry reforming towards products what avoids carbon formation at some extent. Carbon deposition has been detected at temperatures lower than 900 °C. These deposits were partially removed along isothermal experiments, probably by CO_2 (Boudouard), and/or newly formed H_2 and CO (MDR). EDS analysis demonstrated that carbon is mostly formed on the surface of nickel particles, while Raman spectroscopy shows that this carbon was highly graphitized. Metallic iron can be reoxidized with steam in a subsequent stage releasing high purity hydrogen.

1. Introduction

As time goes by energy supply becomes an issue of capital importance worldwide. Currently, most of the energy around the world is still produced from fossil fuels, constituting a non-suitable environmental choice and a questionable bet in a mid and long term future. In this context, hydrogen is rising as a promising alternative to diminish greenhouse emissions and accordingly the climate change; not only because it does not contribute to the carbon fingerprint if produced from renewable sources, but

* Corresponding author. Tel.: +34 976 762390; fax: +34 976 762043.
E-mail address: jap@unizar.es (J.A. Peña).

0016-2361/$ - see front matter © 2013 Elsevier Ltd. All rights reserved.
http://dx.doi.org/10.1016/j.fuel.2013.10.069

because if fed to fuel cells, constitutes an energy vector in transport, one of the most polluting sectors [1].

Several methods are being employed in current hydrogen production. Steam reforming of natural gas followed by purification by pressure or temperature swing adsorption (PSA and TSA) is widely used due to the fact that it is a cheap and mature technology [2]. Coal gasification also falls in the category of proven technologies but with an important drawback regarding its polluting effect [2].

Water electrolysis seems to be a promising alternative provided that electricity needs are covered by renewable sources like solar or wind mill farms during off-peak times. Although the high purity achievable by this method makes it very suitable for PEMFC (e.g. transport and allocated applications), its high price makes this alternative uncertain up to date [2–4].

Thermocatalytic decomposition of methane (natural gas), is another alternative with which high value by-products like carbon nanofibers and nanotubes are foreseen to be co-produced [5]. Other alternatives plan obtaining hydrogen starting from biomass via gasification or pyrolysis [2,6–8]. All of these promising options bear in mind two important aspects: the renewable origin of the source, and the high purity of hydrogen to be achieved. In this sense, the present work is intended for exploring new ways of generation of pure hydrogen starting from another alternative biomass source: biogas [9].

Biogas is produced by the anaerobic digestion of organic matter, such as biomass, municipal solids, and industrial or livestock wastes [10]. Its composition includes mainly CH_4 and CO_2 which accounts for up to 98(vol%) depending on the source [11]. Nitrogen, hydrogen sulphide, siloxanes and steam are also present but in minor proportions [10–12]. Currently the most used method to take profit from this gas consists of burning it in internal combustion engines producing electricity and heat by cogeneration. Taking apart minor components like H_2S and siloxanes that must be removed prior to almost any further treatment, among the main drawbacks for such use can be mentioned the low heating value of the biogas [10] and the knocking properties that might mechanically damage the engines depending on the CH_4/CO_2 ratio [13]. On the other side, methane dry reforming (MDR) seems to be an interesting alternative since taking apart the above mentioned contaminants, the CH_4/CO_2 ratio of the mix can be profitable for producing rich mixtures of H_2 and CO. In this case, an unavoidable task is the further purification of the hydrogen contained in the mixture if it is going to be post-processed in a PEMFC. Moreover, an important drawback of this reaction, pointed out recently by Oyama et al. [14], is that carrying out the reaction at pressures only slightly above atmospheric (5 bar), reverse water gas shift can be drastically promoted, consuming the incipient hydrogen and carbon dioxide to produce carbon monoxide and water. An ideal solution would consist of removing hydrogen as soon as it is produced, substituting it by steam.

To cope with these issues, two coupled processes are being proposed in this work: on the one hand, the catalytic dry reforming of methane [15]. On the other, the steam-iron process originally devoted to produce pure hydrogen for aerial navigation in the early XX century from mixtures resulting from coal gasification [16,17].

Steam-iron process consists ideally of two steps occurring in a cyclic and discontinuous manner. The reduction of iron oxides with a reductive gas to obtain metallic iron or iron in a lower oxidation state (r.1) and (r.2) constitutes the first stage. The second stage consists of the reoxidation of the previously reduced iron with steam (r.3). Hydrogen is then released and iron oxide is regenerated completing the cycle. Several applications as hydrogen production [18,19], hydrogen purification [20,21] and hydrogen storage [22] are possible depending on the composition of the reductive gas.

$$Fe_2O_3 + 3H_2 \rightleftharpoons 2Fe + 3H_2O \quad (r.1)$$

$$Fe_2O_3 + 3CO \rightleftharpoons 2Fe + 3CO_2 \quad (r.2)$$

$$3Fe + 4H_2O \rightleftharpoons Fe_3O_4 + 4H_2 \quad (r.3)$$

In this context, sweetened biogas can behave as reductive source depending on its CH_4 to CO_2 proportion. Nevertheless, methane alone is not able to reduce iron oxide to metallic iron at moderate temperatures (e.g. 500–650 °C) because of thermodynamic limitations [23]. To afford this task it is necessary to favour methane dry reforming (r.4) with the aid of a catalyst which produces H_2 and CO that actually are the potential reducers of iron oxides [24,25]. Since this reaction follows a comparable path to that of steam reforming, same kind of catalysts can be considered to undertake this job [26].

$$CH_4 + CO_2 \rightleftharpoons 2CO + 2H_2 \quad (r.4)$$

According to these authors, the reaction mechanism consists of two steps. The first one corresponds to methane dehydrogenation (r.5), being the second one the gasification of the previously deposited coke by CO_2 (r.6). In both cases the reaction takes place in the surface of the metallic nickel [27].

$$Ni(s) + CH_4 \rightleftharpoons Ni - C(s) + 2H_2 \quad (r.5)$$

$$Ni - C(s) + CO_2 \rightleftharpoons Ni(s) + 2CO \quad (r.6)$$

The most widely used catalyst to carry out this task is nickel supported on alumina. Although metallic iron from reactive solid could act as catalyst, its effect is negligible at the temperature range tested [5]. Nickel crystallites size and dispersion degree along the catalyst surface are key factors in its performance [28]. These characteristics also influence the type and reactivity of the coke eventually formed. Chen et al. [29] established that the higher the size of crystallites, the less probable is the formation of carbon nanotubes or nanofibers, allowing on such way the appearance of important quantities of amorphous carbon that could be more easily gasified than those highly structured. An adequate control of the size of nickel crystallites can lead to a convenient balance between simultaneous coke production and gasification, during dry reforming of biogas. Bulk catalyst based in nickel oxides, with crystallites in the order of hundred microns can be a good candidate.

The main objective of this work has been testing the feasibility of producing as purer hydrogen from a sweetened biogas as could be achieved, by the joint action of two processes taking place in the same reactor. Catalytic methane dry reforming – MDR – (r.4) produces hydrogen which is sequestrated by reducing an iron based oxide (steam-iron) (r.1). Same role plays CO co-produced with H_2 (r.2). After reduction, hydrogen can be released in a further stage by reaction of the metallic iron with steam according to reaction (r.3).

2. Experimental

2.1. Materials

Solid was composed of a mechanical mixture of a reactive one (iron oxide plus additives) and a catalyst (nickel oxide). The composition of the first is the result of a previous research focused on purification of methane pyrolysis gases by the steam-iron process [30,31]. Its main component is Fe_2O_3 (hematite) (98 wt%) which is doped with 1.75(wt%) of Al_2O_3, that stabilizes its mechanical properties and 0.25(wt%) of CeO_2 that promotes its reactivity.

Solids were synthesized separately according to a precipitation method based on citrates [32]. The starting materials were

$Fe(NO_3)_3{\cdot}9H_2O$, $Al(NO_3)_3{\cdot}9H_2O$, $Ce(NO_3)_4{\cdot}6H_2O$ for iron oxide and $Ni(NO_3)_2{\cdot}9H_2O$ for the catalyst, at least 99% purity, all of them from Sigma–Aldrich. A metallic nitrate solution (1 M) was heated to 80 °C and then citric acid solution (1 M) was poured into the beaker. After 2 h stirring, the gel was formed. Then it was dried at 60 °C for 12 h and calcined in two steps: 350 °C for 2 h, and 800 °C for 8 h. Finally, it was crushed and sieved. The selected particle size was 100–160 μm. BET surface was measured for the samples, being 13.7 m^2/g for the doped iron oxide, and as low as 1.2 m^2/g for the NiO.

2.2. Methods

The thermogravimetric analyses (TG) were performed on a *STA 449 F3 Jupiter of Netzsch*® using alumina crucibles as support for the solid. It was operated in stationary and dynamic regime of thermal conditions. In isothermal mode at temperatures ranging from 600 °C to 900 °C and in dynamic conditions from room temperature up to 1000 °C, at a rate of 5 °C/min. It was fed with a reductive atmosphere simulating and ideal composition of biogas of equimolar CH_4/CO_2 ratio diluted in argon. Initial sample weight was 20 mg in all cases, corresponding to a space velocity (WHSV) of 100 h^{-1}. A mass spectrometer (*Pfeiffer, model Omnistar Prisma*) and a μGC (Agilent 490) connected to the TG were used to follow up the evolution of composition of the exhaust gases exiting from the TG system.

XRD analyses of both, fresh and reduced oxides were carried out in a *D-Max Rigaku diffractometer* with Cu anode and graphite monochromator. The range used for the measurements was from 5° to 80°.

SEM images were obtained by a field emission scanning electronic microscopy (FESEM), *Carl Zeiss Merlin* model operating with 5 kV. In addition, the instrument was able to detect the composition of the surface through the energy-dispersive X-ray spectroscopy (EDS). The Raman analyses were carried out in a *Horiba JobinYvon, LabRAM HR UV–VIS NIR*. Raman spectra were recorded with an Ar-ion laser beam at an exciting radiation wavelength of 532 nm.

3. Results and discussion

3.1. Reduction in TG

3.1.1. Non-isothermal reductions

Fig. 1 shows the different behaviours of doped iron oxide, nickel oxide, 50:50 (wt%) mechanical mixture and co-precipitated oxides (also 50:50 wt%) when they are subjected to a typical weight loss experiment. The composition of the gas fed was 12% CH_4 + 12% CO_2 (vol%) diluted in argon at atmospheric pressure. The heating rate adopted in these experiments was 5 °C/min and the sample mass was 20 mg.

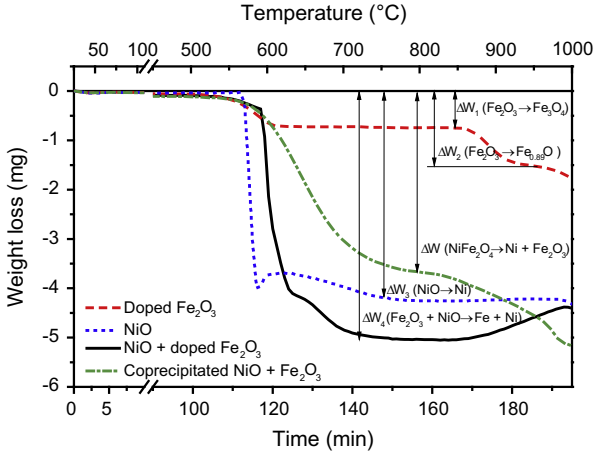

Fig. 1. Weight loss by reduction of species (co-precipitated nickel ferrite, nickel oxide, doped iron oxide and a 50:50 wt%-mixture of both) at a constant heating rate (β = 5 °C/min). A $Fe_{0.89}O$ stoichiometry has been used in ΔW_2 according to empirical results.

As seen in this figure, no significant weight loss or gain was recorded in the range of temperatures below 550 °C. Doped iron oxide reduction begins at 550 °C and continues its transformation into magnetite up to 640 °C. The weight loss according to this step agrees well with the stoichiometric proportion between hematite (Fe_2O_3) and magnetite (Fe_3O_4) (ΔW_1 in Fig. 1). At 865 °C, magnetite reduction progress to wüstite (FeO) ($\Delta W_1 + \Delta W_2$). This sample is unable to reach total reduction ($\Delta W = -6$ mg) even at high temperatures (1000 °C). No evidences of reduction of the minor constituents doping the iron oxide were detected by TGA or XRD.

Pure nickel oxide is reduced to Ni^0 at 586 °C in a single sharp step. After that drop, a weight gain is recorded, probably due to carbonaceous residue formation according to catalytic methane decomposition [5]. This residue is completely gasified afterwards ($\Delta W_3 = -4.3$ mg), probably by CO_2 present in the feed at 800 °C, according to reverse Boudouard reaction (r.6), or by hydrogen according to reverse (r.5). This issue regarding the formation of carbonaceous deposits will be revisited later in this paper.

The behaviour of the mechanical mix of both solids (50:50 wt%) does not represent the sum of both constituents. The mixture reduces first to magnetite and then continues into nickel (Ni^0) and iron (Fe^0) ($\Delta W_4 = -5.1$ mg). As weight loss slows down (something less than −4 mg) it can be observed an unusual change in the slope (small shoulder). This is primarily attributed to carbonaceous residue formation which disappears faster than in the pure nickel oxide reduction experiment. In addition, there is no evidence of wüstite presence as was confirmed by XRD (Fig. 5). Around 855 °C it is produced an increasing weight gain, probably due to the decomposition of methane catalysed by metallic iron [33]. As consequence of the above described phenomena, a synergistic effect was observed in the event of mixtures that cannot be attributed to its constituents separately. For example, carbon deposited at a given temperature in unmixed solids disappears faster or even has no opportunity to be deposited in the mixture. In addition, it is important to note that the doped iron oxide in the mixture can be reduced not only in a greater extent but also at lower temperatures than iron oxide alone. Just for comparison purposes, equivalent analysis was performed on a sample of co-precipitated nickel and iron oxides (nickel ferrite) maintaining the same proportion of metallic oxides than in the experiments performed with mechanical mixtures. Although the sample was

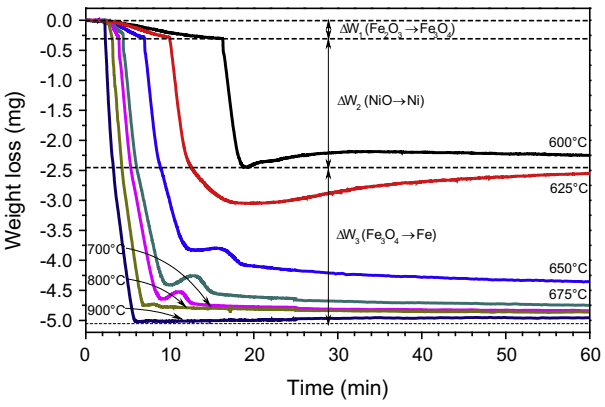

Fig. 2. Weight loss during reduction in isothermal conditions of a mix (50:50 wt%) NiO + doped Fe_2O_3 at several temperatures.

completely reduced, it only could be achieved at temperatures as high as 1000 °C.

3.1.2. Isothermal reductions

The reduction of the mechanical mixture doped Fe_2O_3 + NiO has been tested in isothermal conditions at different temperatures from 600 °C to 900 °C (see Fig. 2).

All curves show a similar behaviour: a first step corresponding to the reduction from hematite to magnetite (ΔW_1), and a second that agrees well with the reduction of NiO to metallic nickel (ΔW_2). Finally, during the last step, magnetite is reduced to metallic iron (ΔW_3). How these steps follow each other strongly varies depending on temperature. At 900 °C, the highest temperature tested, a complete reduction up to stoichiometric weight loss can be recorded. The weight drops almost vertically suggesting that the reduction reaction is so fast that the three above mentioned steps are overlapped. No other phenomena different from the global reduction can be distinguished. On the contrary, when temperature undergoes a slight lowering (e.g. 800 °C), reduction is almost as fast as the one at 900 °C, but when weight is approaching its lowest admissible value, the weight loss suddenly slows down and an incipient slope can be noticed between minutes 6 and 9. Although this prominence disappears after this short period (3 min), the stoichiometric weight floor is never recovered again.

As temperature is diminished, this behaviour is accentuated: the "hill" begins to grow up, being the protuberance taller and wider as long as temperature decreases. The lower the temperature, the slower is the reduction reaction rate, the bigger is the protuberance and the farther is the final weight from the stoichiometric limit.

In the experiment at lowest temperature, the minimum weight observed (around 19 min) coincides with the accumulative weight loss of Fe_2O_3 to Fe_3O_4 transition and the reduction of NiO to Ni^0.

The hypothesis to explain this behaviour could be found in the formation and regasification (total or partial) of carbonaceous deposits over the solid by the reverse Boudouard reaction, which is thermodynamically favoured at temperatures above 400 °C. This issue was also observed in the above mentioned non-isothermal experiments (Fig. 1).

To corroborate this hypothesis, a temperature of 650 °C was selected as standard temperature to obtain more information about the steps proceeding to the complete reduction (Fig. 3). The constituent oxides (NiO and doped iron oxides) were subjected to isothermal experiments separately and compared with the mixture 50:50 (shown in Fig. 2). The behaviour is very close to that found in experiments subjected to a temperature ramp (see Fig. 1): at that temperature, Fe_2O_3 can only be reduced to Fe_3O_4 ($\Delta W = -0.7$ mg), while NiO is reduced to Ni^0 ($\Delta W = -4.3$ mg) through deposition-gasification of carbon.

Exhaust gases of the reduction experiment carried out at 650 °C with the mix of oxides, were analysed in parallel by both, on-line mass spectrometry and gas chromatography (μGC). Fig. 4 shows the evolution of the gaseous species as well as the weight lost by the solid. It has been segmented in several periods labelled from A to E. During period A, reactive gases enter the reaction chamber (at time zero) beginning the reduction of Fe_2O_3 to Fe_3O_4. During this period partial pressures corresponding to CO_2 and CH_4 grow due to flooding of the experimental system previously filled with inert gas (Ar). CH_4 partial pressure always remains lower than that of CO_2 during this period. A local maximum of CH_4 partial pressure agrees well with the beginning of the sharp drop of the sample weight (t = 5.4 min), which starts reducing NiO to Ni^0 and which marks the transition between stage A and B. Note also that H_2 presence has only been detected, as well as that of CO, at the end of period A. An explanation for such behaviour could be that CH_4 is

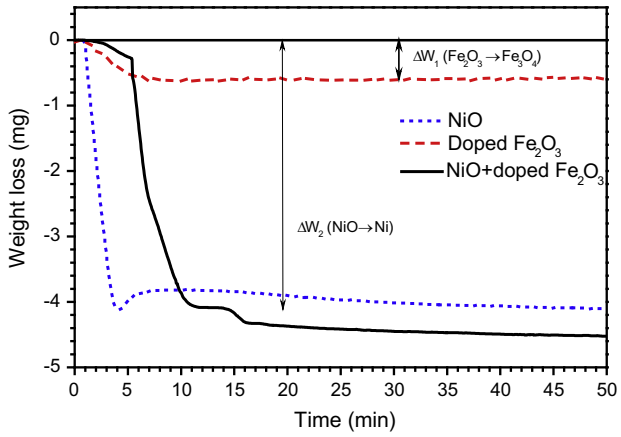

Fig. 3. Reduction of a sample of mixed NiO and doped Fe_2O_3 and its separate components in isothermal conditions (650 °C) with a gaseous equimolar mix (0.24 bar) of CH_4/CO_2 (diluted in Ar).

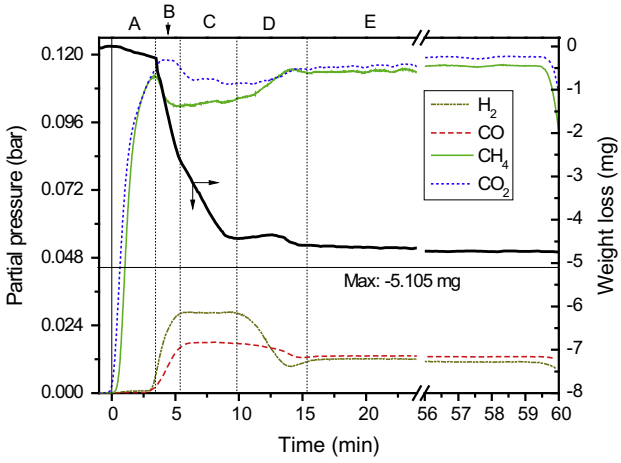

Fig. 4. Partial pressures of gaseous species and weight lost by the solid along time during a reduction at 650 °C of a mix 50:50 (wt%) of NiO + doped Fe_2O_3.

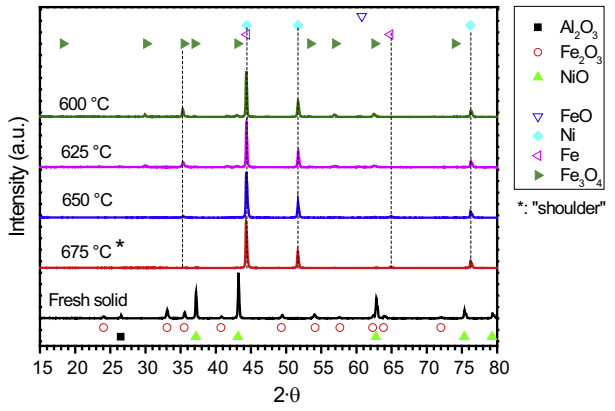

Fig. 5. XRD diffractograms of fresh solid (NiO + doped Fe_2O_3), after reduction at different temperatures (600, 625 and 650 °C) and at the "shoulder" (t = 13 min of Fig. 2) at 675 °C.

mainly being burnt with the lattice oxygen of Fe_2O_3 which reduces to Fe_3O_4 producing CO_2 as gaseous species.

Period B is characterized by an almost linear weight loss where NiO is reduced to Ni^0. In this case, CO and H_2 signals pass from an almost constant null value to an intense rise. Again, CH_4

combustion by the oxygen of NiO seems to be the most likely reason. Simultaneously, CH_4 partial pressure decreases because it is consumed in the reaction while CO_2 stabilizes. The reason might be found in the fact that along this period, newly formed Ni^0 promotes the formation of CO and H_2 by methane dry reforming (r.4).

Along period C it seems probable that the reduction of the magnetite to metallic iron is taking place at the expense of hydrogen and probably also from CO. Both components exhibit constant partial pressures as consequence of the catalytic MDR.

Period D begins with the stabilization of the weight and with the fall of H_2 signal. CO partial pressure also falls but in a slowly manner. Catalytic MDR is slowing down, probably because a carbonaceous residue is covering the actives sites of nickel crystallites reducing its catalytic activity. Also a gasification of the previously deposited coke takes place in this period, as evidenced by the elimination of the protuberance exhibited from minutes 11 to 15 in the weight loss curve.

Period E corresponds to a stable regime where partial pressures of CH_4 and CO_2 are almost constant, with a residual activity which generates a low but stable concentration of H_2 and CO. Finally, inert gas was commuted (at around 60 min) being all signals reduced to zero (not shown).

It is necessary to clarify at this point that the main scope of this isothermal experiment was to show the behaviour of the different gaseous species rather that maximize the reactants conversion. In this context, the TG apparatus is being operated as a differential reactor what explains the low conversion of reactives.

3.2. Solids characterization

3.2.1. XRD analysis

Diffractograms for fresh solid mixtures and for solid after the first reduction run are shown in Fig. 5. For fresh solid, it has been identified the presence of peaks corresponding to Fe_2O_3, NiO and Al_2O_3. No ceria signal was observed probably due to the small mass fraction content in the oxide (0.25 wt%).

Samples of solid previously reduced at temperatures of 600 °C, 625 °C and 650 °C were also analysed. At these temperatures, metallic Ni and Fe are the main species detected verifying that the reduction has taken effect. This fact is especially evident at the highest temperature (650 °C), where no other oxides were detected. On the other side, as long as temperature is decreased, the presence of oxidized iron (Fe_3O_4) becomes patent. No evidences of crystalline carbon (26° pattern) or FeO (wüstite) have been detected. This fact might be attributed to a limited crystallization (amorphous carbon), a small content in the sample or to both reasons.

Diffractogram labelled as 675 °C* was carried out over a sample stopped at the local maximum weight at such temperature (e.g. at a time t = 13 min in Fig. 2) in order to detect possible coke formation. No evidences of such carbon were either detected by this method.

3.2.2. SEM–EDS analysis

Samples of solid after reduction at 600 °C can be visualized in Fig. 6. The main purpose for this analysis consisted of determining if significant amounts of carbon could be detected by EDS in samples of solids subjected to regular isothermal conditions at the above mentioned temperature. This last was selected according to the behaviour shown in Fig. 2, trying to capture the shoulder at 60 min produced during the reduction process. Since the mixing method for the production of the final solid is a mere mechanical mixture, images could be focused on particles of different composition (iron based or nickel based) within the sample. Thus, EDS analysis was performed in two points labelled as Point 1 and Point 2 at Fig. 6. Both have been selected as representatives of iron and

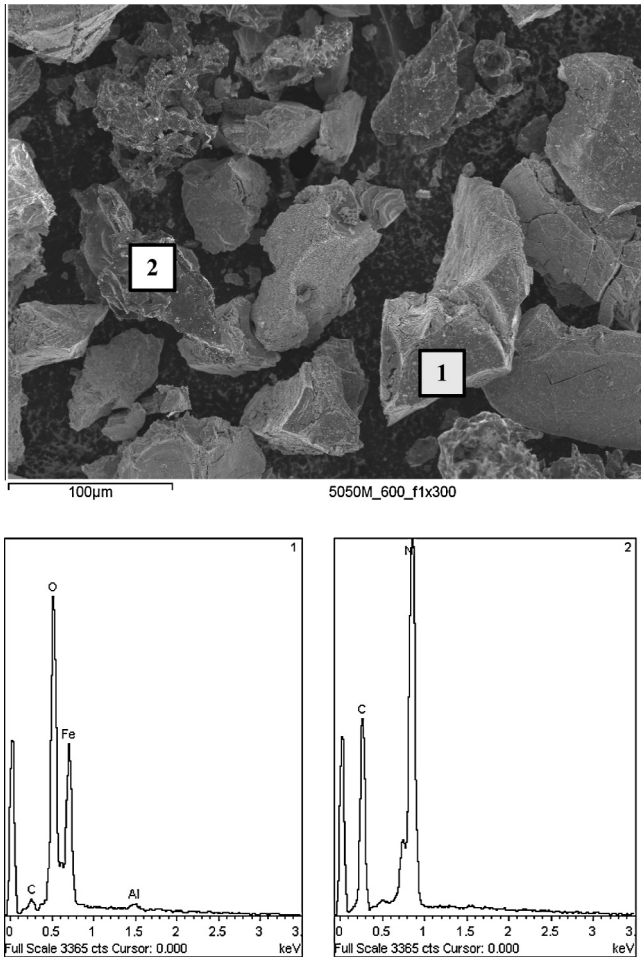

Fig. 6. FESEM image and EDS analysis of solid mix after reduction (60 min) at 600 °C.

nickel oxide particles respectively after sampling several points with almost identical values.

Point 1 corresponds to an iron oxide particle. Oxygen, iron and aluminium presence was detected. Also a carbon signal attributed to an interference of the instrument could be envisaged with a maximum between 0.2 and 0.3 keV. Point 2 refers to a nickel oxide particle. Main elements detected are nickel and a higher carbon signal than that found in point 1. It can be concluded that carbon deposition mainly occurs on nickel surface, according to typical deactivation of nickel catalyst on reforming processes [34]. In order to determine the quality of the carbon deposited, Raman analysis were also performed on the samples.

3.2.3. Raman analysis

Although EDS evidenced the presence of carbon deposits associated to particles of nickel (Fig. 6), XRD analysis could not confirm the presence of crystalline carbon (see Fig. 5). Raman analysis has been used to this point to determine the nature of the carbon deposited on the sample. Since it is composed of a mechanical mixture of different solids (nickel oxide + doped iron oxide), this kind of analysis could evidence a heterogeneous distribution of the carbon deposited on the constituent solids.

Fig. 7 shows the results of Raman analysis performed on a solid that was reduced at 650 °C with the regular mixture of CH_4/CO_2 equimolar ratio. Such reduction was stopped at the maximum carbon content (at 16 min in Fig. 2). Upper curve shows the spectra of an iron oxide particle with characteristic peaks (marked with

triangles) corresponding to α-Fe_2O_3 [35,36]. Although Fe_2O_3 should not be present in the sample due to the high degree or reduction achieved, its presence could be justified by the post-treatment after cooling and the manipulation in air at ambient temperature prior to the Raman analysis that could lead to a superficial oxidation of the sample. No presence of carbon was evidenced in this particle in any case.

The lower curve in the same figure represents the spectra of a nickel particle. In contrast with that of iron oxide, this clearly shows the presence of carbon with its characteristic D (1353 cm^{-1}) and G (1581 cm^{-1}) bands. The relatively low value of the D respecting G band implies a high degree of graphitization [37]. This fact, joined to the inexistence of XRD peaks related to graphitic carbon lead to conclude that carbon might only be deposited in an outer layer of the nickel particle, forming a kind of encapsulating structure along the nickel surface. Thus, coke would be responsible of deactivating the catalytic effect of the nickel particles by fouling of their active sites. This eventual decrease in the number of available active sites could lead to a slowdown in the CH_4 decomposition and dry reforming rates, as well as to increase the Boudouard reaction rate, responsible for the regasification of the carbon deposits.

3.3. Oxidation with steam

Non-isothermal oxidations with steam (H_2O diluted in Ar at 50vol%), were performed over samples previously subjected to an isothermal reduction stage. Pressure was always atmospheric. The reduction, prior to the oxidation stage, consisted of the exposition of the regular solid sample (50:50 wt% NiO + doped Fe_2O_3) to a reductive atmosphere composed of 12% CH_4, 12% CO_2, 76% Ar (vol%) at a temperature of 650 °C for 1 h.

Fig. 8 shows the weight increase of the solid (right axis) and the hydrogen partial pressure in the stream coming out from the thermogravimetric system (left axis) along time or temperature. The weight of the solid mixture exhibits an inflection point (maximum weight increase rate) at a temperature of 500 °C. This maximum agrees well with the maximum value achieved in the H_2 partial pressure. It has also been calculated that the area under the peak of hydrogen production agrees well (5% error) with the corresponding amount of iron oxide (Fe_3O_4) produced by reaction (r.3). Although CO_2 and CO were detected by MS, their content was well below the detection limit of the μGC (lower than 5 ppm and 7 ppm for CO_2 and CO respectively) used to calibrate the concentration of gaseous species, so they have not been included in the figure. As consequence, although there is evidence of the carbonaceous deposits generated during the previous reduction step

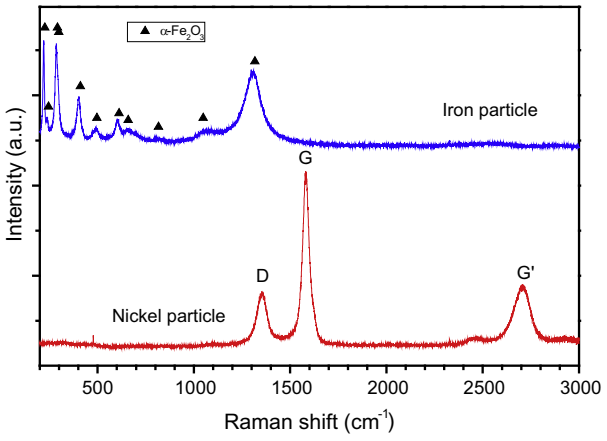

Fig. 7. Raman spectra of solid (nickel and iron particles) after reduction at 650 °C.

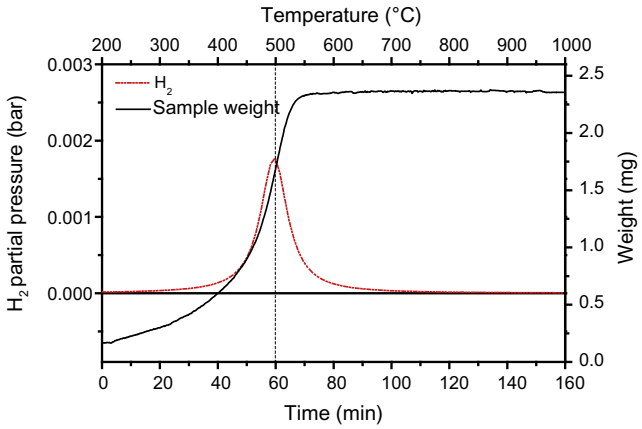

Fig. 8. Solid weight gain (continuous line) and hydrogen partial pressure (dotted line) during the oxidation with steam in a temperature ramp ($\beta = 5$ °C) after previous reduction at 650 °C.

(roughly 6% of the sample weight @ 700 °C), the oxidation reaction (r.3) produces a stream of hydrogen pure enough to be fed to a PEMFC.

4. Conclusions

Mechanical mixtures of nickel oxide and iron oxide doped with ceria and alumina have been tested in order to produce rich hydrogen streams starting from mixtures of CH_4 and CO_2. The main goal was producing as purer hydrogen as possible from a biogas from which sulphur and siloxanes have been conveniently removed. Equimolar mixtures or CH_4 and CO_2 were selected for such purpose.

Nickel oxide acts as catalyst for the dry reforming of methane by carbon dioxide, while doped iron oxide adopts a role of hydrogen and carbon monoxide consumer as long as these reductive species are produced. In a subsequent stage, the previously reduced iron oxide can be regenerated by oxidation with steam, producing high purity hydrogen with low proportions (not appreciable by μGC) of contaminants like CO_x. Additionally, the result of this combination of solids is the displacement of the equilibrium reaction of dry reforming towards products (hydrogen and carbon monoxide), and the inhibition of coke deposits formation to a certain extent.

The use of non-isothermal thermogravimetry over the solid sample, coupled to mass spectrometry for the analysis of the exhaust gases suggests that the most probable sequence of stages consists of the reduction of hematite to magnetite by combustion of methane with the lattice oxygen of the solid, followed by the reduction of nickel oxide by the same mechanism. The appearance of the resulting metallic nickel plays an active role in the reaction of dry reforming of methane which generates reductive species (H_2 and CO) capable of reducing magnetite to metallic iron through wüstite.

Carbon deposition followed by gasification has been observed during the reduction steps in isothermal experiments carried out by thermogravimetry at temperatures up to 900 °C. At this temperature also a complete reduction of the solids (up to stoichiometric limit) has been achieved. For lower temperatures (from 800 °C down), growing amounts of carbon deposits have been noticed followed by subsequent gasification. The greater is the amount of carbon deposited on the solid surface, the further is the final weight of the iron oxide sample from that of the theoretical (stoichiometric) maximum weight loss achievable by reduction. Coke formed, which has a high degree of graphitization as evidenced by Raman

spectroscopy, is mainly deposited over nickel particles producing some deactivation on the dry reforming reaction along time.

Reduced samples with appreciable quantities of coke were subjected to an oxidation step with steam showing that maximum rates of hydrogen release can be measured at temperatures around 500 °C. Carbon dioxide and carbon monoxide were detected at these temperatures by MS but not by μGC (below its detection limit), concluding that the coke formed behaves as inert respecting steam at this temperature.

It can be stated that results concerning this process are promising, and that more experiments must be carried out in order to determine reaction kinetics and finally the economic balance of the whole process. Preliminary ones foresee a certain margin for the exploitation of poor biogas (e.g. low CH_4/CO_2 ratio) as hydrogen source.

Acknowledgments

Financial support for this research has been provided by the Spanish *Ministerio de Ciencia e Innovación* (MICINN) through project ENE2010-16789. J. Plou also thanks the same institution for the grant BES-2011-045092. Financial aid for the maintenance of the consolidated research group CREG has been provided by the *Fondo Social Europeo* (FSE) through the *Gobierno de Aragón* (Aragón, Spain).

References

[1] U.S. DOE. An integrated strategic plan for the research, development and demonstration of hydrogen and fuel cell technologies. U.S. Department of Energy; 2011.
[2] Holladay JD, Hu J, King DL, Wang Y. An overview of hydrogen production technologies. Catal Today 2009;139(4):244–60.
[3] Bartels JR, Pate MB, Olson NK. An economic survey of hydrogen production from conventional and alternative energy sources. Int J Hydrogen Energy 2010;35(16):8371–84.
[4] Lattin WC, Utgikar VP. Transition to hydrogen economy in the United States: a 2006 status report. Int J Hydrogen Energy 2007;32(15):3230–7.
[5] Li Y, Li D, Wang G. Methane decomposition to COx-free hydrogen and nano-carbon material on group 8–10 base metal catalysts: a review. Catal Today 2011;162(1):1–48.
[6] Bohn CD, Muller CR, Cleeton JP, Hayhurst AN, Davidson JF, Scott SA, et al. Production of very pure hydrogen with simultaneous capture of carbon dioxide using the redox reactions of iron oxides in packed beds. Ind Eng Chem Res 2008;47(20):7623–30.
[7] Bertero M, de la Puente G, Sedran U. Fuels from bio-oils: bio-oil production from different residual sources, characterization and thermal conditioning. Fuel 2012;95(1):263–71.
[8] National Renewable Energy Laboratory. Hydrogen production cost estimate using biomass gasification. 2011 [Contract No.: NREL/BK-6A10-51726].
[9] Alves HJ, Bley Junior C, Niklevicz RR, Frigo EP, Frigo MS, Coimbra-Araújo CH. Overview of hydrogen production technologies from biogas and the applications in fuel cells. Int J Hydrogen Energy 2013;38(13):5215–25.
[10] Deublein D, Steinhauser A. Biogas from waste and renewable resources. An introduction. Wiley VCH; 2008.
[11] Wellinberg A, Lindberg A. Biogas upgrading and utilisation. International Energy Agency; 2001.
[12] Demirbas A. Biohydrogen for future engine fuel demands. Springer Verlag; 2009.
[13] Sahoo BB, Sahoo N, Saha UK. Effect of engine parameters and type of gaseous fuel on the performance of dual-fuel gas diesel engines – a critical review. Renewable Sustainable Energy Rev 2009;13(6-7).
[14] Oyama ST, Hacarlioglu P, Gu Y, Lee D. Dry reforming of methane has no future for hydrogen production: comparison with steam reforming at high pressure in standard and membrane reactors. Int J Hydrogen Energy 2012;37(13).
[15] Fan M-S, Abdullah AZ, Bhatia S. Catalytic technology for carbon dioxide reforming of methane to synthesis gas. Chem Cat Chem 2009;1(2).
[16] Messerschmitt A. Process of producing hydrogen. U.S. Patent 971; 1910.
[17] Hacker V, Fankhauser R, Faleschini G, Fuchs H, Friedrich K, Muhr M, et al. Hydrogen production hy steam-iron process. J Power Sources 2000;86(1-2).
[18] Hacker V, Faleschini G, Fuchs H, Fankhauser R, Simader G, Ghaemi M, et al. Usage of biomass gas for fuel cells by the SIR process. J Power Sources 1998;71(1-2).
[19] Hacker V, Fuchs H, Fankhauser R, Spreitz B, Friedrich K, Faleschini G. Hydrogen production from gasified biomass by sponge iron reactor (SIR). Hydrogen Energy Progress XII 1998:1–3.
[20] Lorente E, Peña JA, Herguido J. Kinetic study of the redox process for separating and storing hydrogen: oxidation stage and ageing of solid. Int J Hydrogen Energy 2008;33(2):615–26.
[21] Lorente E, Cai Q, Peña JA, Herguido J, Brandon NP. Conceptual design and modeling of the steam-iron process and fuel cell integrated system. Int J Hydrogen Energy 2009;34(13):5554–62.
[22] Thaler M, Hacker V. Storage and separation of hydrogen with the metal steam process. Int J Hydrogen Energy 2012;37(3):2800–6.
[23] Peña JA, Ferreira V, Marin A, Durán P, Romero E, Herguido J. Obtaining pure hydrogen from natural gas pyrolysis by redox processes. In: 18th World hydrogen energy conference (WHEC2010). Essen (Germany); 2010.
[24] Jozwiak WK, Kaczmarek E, Maniecki TP, Ignaczak W, Maniukiewicz W. Reduction behavior of iron oxides in hydrogen and carbon monoxide atmospheres. Appl Catal A-Gen 2007;326(1):17–27.
[25] Pineau A, Kanari N, Gaballah I. Kinetics of reduction of iron oxides by H-2 - Part I: low temperature reduction of hematite. Thermochim Acta 2006;447(1):89–100.
[26] Wei JM, Iglesia E. Isotopic and kinetic assessment of the mechanism of reactions of CH_4 with CO_2 or H_2O to form synthesis gas and carbon on nickel catalysts. J Catal 2004;224(2):370–83.
[27] Verykios XE. Catalytic dry reforming of natural gas for the production of chemicals and hydrogen. Int J Hydrogen Energy 2003;28(10):1045–63.
[28] Rostrup-Nielsen JR. Catalytic Steam Reforming. J.R. Anderson MB, editor. Berlin: Springer Verlag; 1984.
[29] Chen D, Christensen KO, Ochoa-Fernandez E, Yu ZX, Totdal B, Latorre N, et al. Synthesis of carbon nanofibers: effects of Ni crystal size during methane decomposition. J Catal 2005;229(1).
[30] Lorente E, Peña JA, Herguido J. Separation and storage of hydrogen by steam-iron process: effect of added metals upon hydrogen release and solid stability. J Power Sources 2009;192(1):224–9.
[31] Peña JA, Palacios A, Martínez L, Romero E, Durán P, Herguido J, editors. Effect of impurities of the solid on the subsequent hydrogen release in steam-iron process. In: 18th World hydrogen energy conference 2010 - WHEC 2010. Essen (Germany): Forschungszentrum Jülich GmbH, Zentralbibliothek, Verlag; 2010.
[32] Kirchnerova J, Alifanti M, Delmon B. Evidence of phase cooperation in the $LaCoO_3$-CeO_2-Co_3O_4 catalytic system in relation to activity in methane combustion. Appl Catal A-Gen 2002;231(1–2):65–80.
[33] Pinilla JL, de Llobet S, Suelves I, Utrilla R, Lázaro MJ, Moliner R. Catalytic decomposition of methane and methane/CO_2 mixtures to produce synthesis gas and nanostructured carbonaceous material. Fuel 2011;90(6):2245–53.
[34] Peña JA, Herguido J, Guimon C, Monzon A, Santamaria J. Hydrogenation of acetylene over Ni/$NiAl_2O_4$ catalyst: characterization, coking, and reaction studies. J Catal 1996;159(2).
[35] Luebbe M, Gigler AM, Stark RW, Moritz W. Identification of iron oxide phases in thin films grown on Al_2O_3 (0001) by Raman spectroscopy and X-ray diffraction. Surf Sci 2010;604(7-8).
[36] Caudron E, Tfayli A, Monnier C, Manfait M, Prognon P, Pradeau D. Identification of hematite particles in sealed glass containers for pharmaceutical uses by Raman microspectroscopy. J Pharm Biomed Anal 2011;54(4).
[37] Ferrari AC, Robertson J. Interpretation of Raman spectra of disordered and amorphous carbon. Phys Rev B 2000;61(20).